ACS APPLIED MATERIALS & INTERFACES

Research Article

www.acsami.org

Co-Rich ZnCoO Nanoparticles Embedded in Wurtzite $Zn_{1-x}Co_xO$ Thin Films: Possible Origin of Superconductivity

Yu-Jia Zeng,*[,†,‡,§] Nicolas Gauquelin,[∥] Dan-Ying Li,[‡] Shuang-Chen Ruan,[†] Hai-Ping He,[§] Ricardo Egoavil,[∥] Zhi-Zhen Ye,[§] Johan Verbeeck,[∥] Joke Hadermann,[∥] Margriet J. Van Bael,[‡] and Chris Van Haesendonck*[,‡]

[†]Shenzhen Key Laboratory of Laser Engineering, College of Optoelectronic Engineering, Shenzhen University, Shenzhen, 518060, People's Republic of China

[‡]Solid State Physics and Magnetism Section, KU Leuven, Celestijnenlaan 200 D, BE-3001 Leuven, Belgium

[∥]Electron Microscopy for Materials Science (EMAT), University of Antwerp, Groenenborgerlaan 171, BE-2020 Antwerp, Belgium

[§]State Key Laboratory of Silicon Materials, Department of Materials Science and Engineering, Zhejiang University, Hangzhou 310027, People's Republic of China

Supporting Information

ABSTRACT: Co-rich ZnCoO nanoparticles embedded in wurtzite $Zn_{0.7}Co_{0.3}O$ thin films are grown by pulsed laser deposition on a Si substrate. Local superconductivity with an onset T_c at 5.9 K is demonstrated in the hybrid system. The unexpected superconductivity probably results from Co^{3+} in the Co-rich ZnCoO nanoparticles or from the interface between the Co-rich nanoparticles and the $Zn_{0.7}Co_{0.3}O$ matrix.

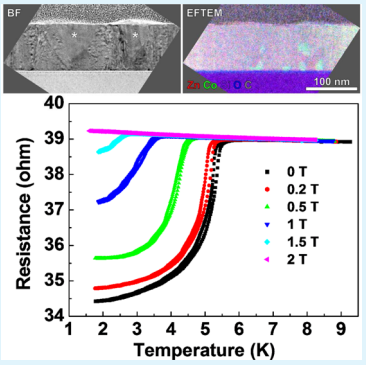

KEYWORDS: *superconductivity, ZnCoO, nanoparticles, ZnO, wurtzite*

INTRODUCTION

Being discovered more than a century ago, superconductivity, the intriguing phase of paired electrons leading to the resistance-free flow of electrical charges, remains a worldwide research focus. In particular, finding a new superconducting material remains most exciting. The discovery of superconductivity in layered copper-based oxides[1] and layered iron-based materials[2] has pushed the transition temperature T_c up to unprecedented high temperatures when compared to the T_c of conventional superconductors. Although there is general consensus on the unconventional nature of the Cooper pairing state, several questions still remain related to the physical origin of high T_c superconductivity. In particular, the discovery of iron-based superconductors was completely surprising because the antagonistic relationship between superconductivity and magnetism has led researchers to avoid using magnetic elements, in particular, ferromagnetic elements, as a building block for new superconductors.[3] In contrast to iron-based superconductors, which became a big family after their discovery,[4,5] cobalt-based superconductors appear quite rare.[6,7] On the other hand, unconventional superconductivity has also been demonstrated at the interface between two insulating oxides, i.e., $LaAlO_3$ and $SrTiO_3$[8−10] or at the electric-field-induced interface in double-layer transistors.[11,12]

Hexagonal wurtzite ZnO, by virtue of its excellent properties, including a wide direct band gap of 3.37 eV at room temperature, a large exciton binding energy of 60 meV, the availability of high-quality bulk crystals, as well as high electron mobility and high thermal conductivity, has been a common host for various doping, in particular, electrical, optical, and magnetic doping.[13,14] However, wurtzite ZnO has never been considered as a building block for superconductors. Here, we report local superconductivity in Co-rich ZnCoO nanoparticles embedded in wurtzite $Zn_{1-x}Co_xO$ thin films with an onset T_c at 5.9 K. The Co-rich ZnCoO nanoparticles, although their microstructure remains to be conclusively determined, are believed to play a key role in the unexpected appearance of superconductivity.

Received: April 30, 2015
Accepted: September 21, 2015
Published: September 21, 2015

DOI: 10.1021/acsami.5b06363
ACS Appl. Mater. Interfaces 2015, 7, 22166−22171

RESULTS AND DISCUSSION

$Zn_{1-x}Co_xO$ thin films are grown by the pulsed laser deposition (PLD) method. Figure 1 presents the X-ray diffraction (XRD)

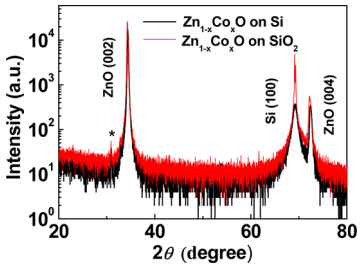

Figure 1. XRD pattern of the $Zn_{1-x}Co_xO$ thin films grown on a Si and on a SiO_2 substrate. The small peak marked with an asterisk results from the high doping of the Si.

patterns of the $Zn_{1-x}Co_xO$ thin films grown on a Si substrate and on a SiO_2 substrate. In both cases only the peaks that correspond to the (002) and (004) planes of wurtzite ZnO are observed, indicating that the $Zn_{1-x}Co_xO$ thin films crystallize in the hexagonal wurtzite structure with strong (002) preferential orientation. No phase separation is detected by XRD even when the nominal Co concentration is as high as 30 atom %. In addition, the local chemical environment of Co was characterized by X-ray absorption near edge structure (XANES) and extended X-ray absorption fine structure (EXAFS). In Figure 2a we present the XANES spectra of the Co K edge for the $Zn_{1-x}Co_xO$ thin film as well as for CoO and Co reference samples. The XANES of the $Zn_{1-x}Co_xO$ resembles the spectrum of CoO rather than that of Co, indicating that the Co is in an oxidized state. In particular, the

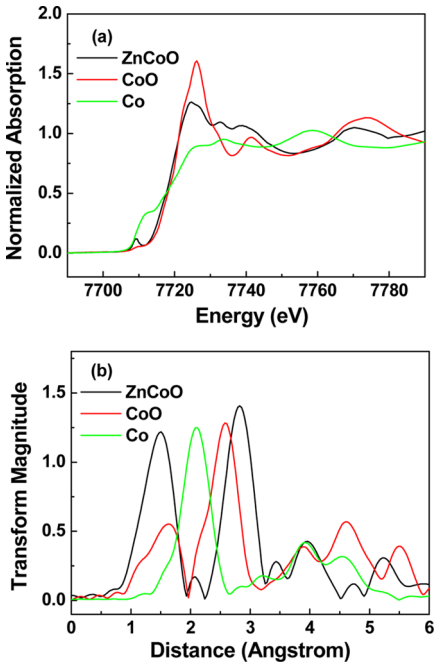

Figure 2. (a) Co K-edge XANES spectra of Co-implanted ZnO thin films of CoO and Co metal. (b) Magnitude of the k^2-weighted Fourier transforms of the EXAFS spectra. For clarity, the magnitude of CoO and Co is multiplied by 0.5 and 0.3, respectively. CoO and Co reference samples are taken from reference 15.

appearance of a small pre-edge absorption at 7709 eV is ascribed to transitions of Co 1s electrons to 4p−3d hybridized states, which become allowed by the nearly tetrahedral bonding of Co at the Zn sites within the wurtzite structure.[15] In Figure 2b we plot the magnitude of the k^2-weighted Fourier transforms of the EXAFS spectra. The $Zn_{1-x}Co_xO$ spectrum reveals two peaks related to the first O shell and the second Zn shell in the wurtzite model. This indicates that the Co atoms are located at Zn sites. We therefore conclude the majority of Co atoms are substitutional on the Zn site in the $Zn_{1-x}Co_xO$ thin film.

The microstructures of the $Zn_{1-x}Co_xO$ thin films grown on both Si and SiO_2 were investigated in detail using transmission electron microscopy (TEM). In Figure 3 we present bright-field

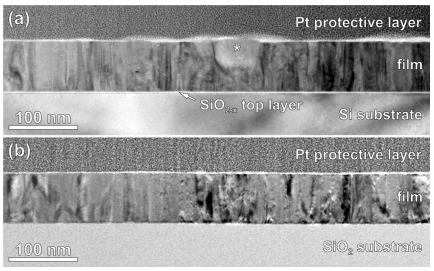

Figure 3. Bright field TEM images of the $Zn_{1-x}Co_xO$ thin films grown on a Si substrate (a) and on a SiO_2 substrate (b).

TEM images of the samples. Both films are polycrystalline with well-pronounced columnar microstructure. The lateral dimensions of the crystallites vary from a few to tens of nanometers. Note that a thin layer of SiO_2 with a thickness of about 2 nm is formed on top of the Si substrate, which is due to the presence of the partial oxygen atmosphere and/or of oxygen diffusion during the film growth. Nevertheless, the microstructure of the thin film grown on the Si substrate differs from that grown on the SiO_2 substrate. The former contains some crystallites violating the regular columnar microstructure (marked with an asterisk in Figure 3a). Electron diffraction (ED) patterns outside of the grain marked with an asterisk (Figure S1 in the Supporting Information) and on that grain (Figure S2 in the Supporting Information) both suggest a hexagonal wurtzite structure. The ED data (Figure S1 in the Supporting Information) demonstrate that the wurtzite c axis is normal to the thin-film surface, which is consistent with the XRD result. On the other hand, the c axis of the grain marked with an asterisk is significantly inclined with respect to the film surface normal by about 25°.

Another significant difference between the samples prepared on the different substrates is that they exhibit a different Co distribution. According to the energy-dispersive X-ray spectroscopy (EDX) analysis, the overall Co concentration is 30 ± 1 and 32 ± 1 atom % for the thin film deposited on the Si substrate and on the SiO_2 substrate, respectively, which is in very good agreement with the composition of the PLD target (x = 0.3 ± 0.01). However, the Co distribution is not homogeneous in the sample grown on the Si substrate. Figure 4 presents the elemental distribution maps for the sample on the Si substrate acquired using the scanning TEM-electron energy loss spectroscopy (STEM-EELS) technique. A Co-rich nanoparticle is clearly present in the $Zn_{1-x}Co_xO$ matrix. According to the EDX data, the Co concentration in the Co-rich region increases to 50 atom %. This value may be underestimated because the Co-rich nanoparticles are tightly embedded in the

DOI: 10.1021/acsami.5b06363
ACS Appl. Mater. Interfaces 2015, 7, 22166−22171

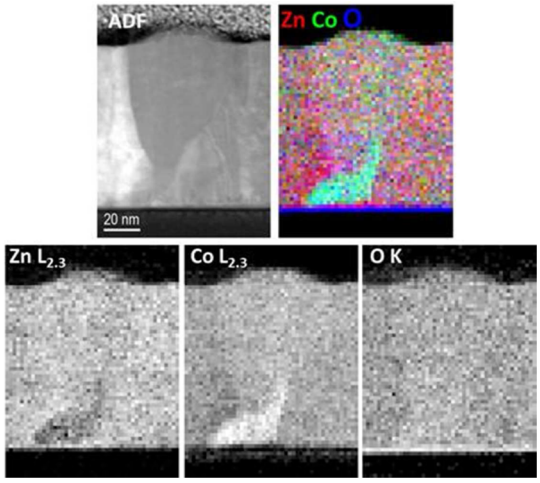

Figure 4. Annular dark field image of the $Zn_{1-x}Co_xO$ thin film grown on a Si substrate and the corresponding elemental maps acquired using EELS spectral imaging at the Zn $L_{2,3}$, Co $L_{2,3}$, and O K absorption edges.

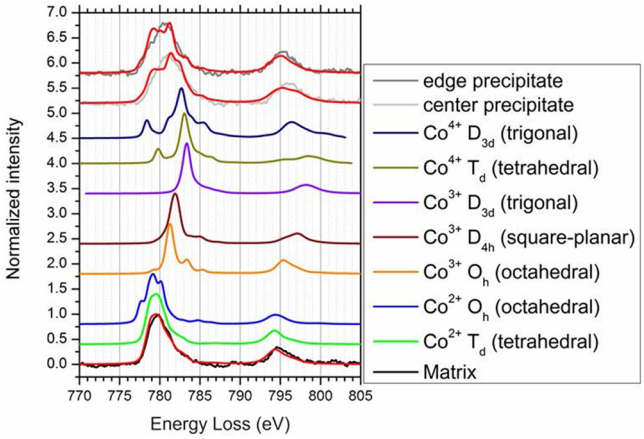

Figure 5. Monochromated STEM-EELS measurements of the Co $L_{2,3}$ edge for the $Zn_{1-x}Co_xO$ matrix (black) and for the center (light gray) and edge (dark gray) of the Co-rich nanoprecipitate with their corresponding fits in red as well as the simulated spectra for Co^{2+} in T_d and O_h, Co^{3+} in O_h, D_{4h}, and D_{3d}, and Co^{4+} in T_d and D_{3d} symmetries.

matrix. The concentration of Co in the surrounding matrix does not significantly deviate from the average concentration. More energy-filtered transmission electron microscopy (EFTEM) maps can be found in the Supporting Information (Figure S3), revealing the presence of the Co-rich nanoparticles at different locations. However, the microstructure of the Co-rich nanoparticles cannot be conclusively determined due to their small size and the big overlap with the matrix. In addition, within the resolution of the measurement (~5 nm) and the accuracy of EELS quantification (~5%), no significant change of the oxygen concentration is observed in the Co-rich regions. This is in contrast to what we recently observed in high-fluence Co-implanted ZnO, in which the Co-rich nanoparticles are metallic.[15,16] Note that no Co-rich nanoparticles are observed in the sample grown on the SiO_2 substrate, i.e., Co is evenly distributed (Figure S4 in the Supporting Information). Therefore, the misaligned grains discussed above are believed to play a key role in the formation of the Co-rich nanoparticles, probably by strain release.

The oxidation states of Co in the $Zn_{1-x}Co_xO$ matrix and in the Co-rich nanoparticles were investigated using monochromated STEM-EELS measurements and multiplet simulations,[17] as illustrated in Figure 5. The parameters for the simulations are reported in Table S1 in the Supporting Information. A nonbiased linear combination of the simulated spectra was used to determine the composition of the matrix and of the Co-rich nanoparticles in 10 different regions of 5 × 4 and 2 × 2 pixels, respectively (Figure S5 in the Supporting Information). The Co valence in the $Zn_{1-x}Co_xO$ matrix is determined to be +2.13, which is fully consistent with the wurtzite structure. The result revealed that 85% of the Co^{2+} is in the tetrahedral (T_d) symmetry with 10% of Co^{3+} in the O_h symmetry, confirming the substitutional character of Co on Zn sites in the $Zn_{1-x}Co_xO$ matrix. The components Co^{2+} in O_h and Co^{3+} in D_{3d} (trigonal) weights are within the experimental error. Assuming that Co^{2+} T_d is only present in the matrix, we can remove the underlying matrix in each spectrum from the precipitate region (after fitting). The oxidation state of Co in the center of the Co-rich nanoparticles is determined to be +2.62 in the same way (49% Co^{3+} O_h, 39% Co^{2+} O_h, and 13% Co^{3+} D_{3d} (trigonal)), whereas the edge regions of the particles present a slightly higher oxidation state of +2.82 (67% Co^{3+} O_h, 19% Co^{2+} O_h, and 14% Co^{3+} D_{3d}). The presence of Co^{3+} D_{3d} at both the sides and the center of the precipitate could be explained by the presence of these ions along the interface between the matrix and the precipitate. The core of the precipitate contains Co^{2+} and Co^{3+} in O_h symmetry. The variation of the Co^{2+}/Co^{3+} ratio in octahedral sites, which is observed between the edges and the center of the region where the nanoprecipitate is present, might be the result of the presence of a gradient of composition from the center to the surface of the precipitate from Co^{3+}/Co^{2+} = 1.5 to Co^{3+}/Co^{2+} = 4. One exemplary fitted spectrum for the center and the edge of the precipitate can be found in Figure 5, and the related parameters can be found in Table S2 in the Supporting Information.

Now we demonstrate the presence of local superconductivity which we relate to the presence of the Co-rich nanoparticles. In Figure 6a we present the temperature dependence of the resistance of the $Zn_{1-x}Co_xO$ thin film grown on a Si substrate under different magnetic fields parallel to the thin-film surface. Note that the resistance is expected to include the resistance of the Co-rich nanoparticles as well as of the $Zn_{1-x}Co_xO$ matrix. Despite the large residual resistance, which can be associated with the nonsuperconducting regions of the thin film, we clearly observe an onset T_c at 5.9 K for both decreasing and increasing temperature. Note that such a nonzero resistance has also been observed in other superconductors, including $Na_xCoO_2{\cdot}yH_2O$[6] and $ZrZn_2$.[18] The applied magnetic field shifts T_c toward lower temperatures. A magnetic field of 2 T completely destroys the superconducting state in the accessible temperature range. A perpendicular magnetic field results in a similar shift of T_c toward lower temperatures. In Figure 6b we compare the critical field as a function of temperature for the parallel and perpendicular field geometries. The critical field for $T \rightarrow 0$ is estimated by linear extrapolation from the phase diagram to be 2.8 and 2.5 T for the parallel and perpendicular geometries, respectively. From the linear slopes of the critical field curves near T_c we infer values of the zero temperature superconducting coherence length of 10 and 11 nm for the parallel and perpendicular geometries, respectively, according to the equation[19]

DOI: 10.1021/acsami.5b06363
ACS Appl. Mater. Interfaces 2015, 7, 22166−22171

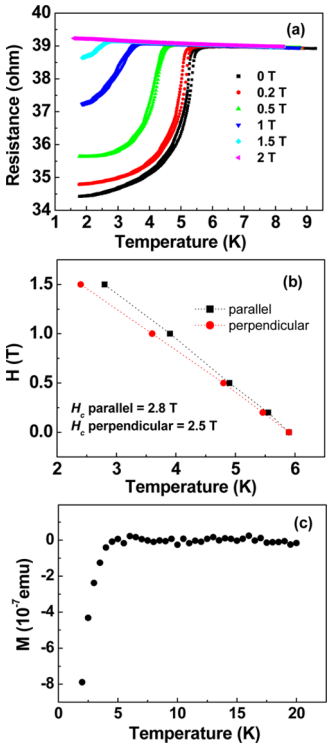

Figure 6. Superconducting properties of the $Zn_{1-x}Co_xO$ thin film grown on a Si substrate. (a) Temperature dependence of the resistance for different magnetic fields parallel to the thin-film surface. (b) Critical field as a function of temperature for the parallel and perpendicular geometries. (c) Temperature dependence of the magnetization measured at a magnetic field of 0.1 T in a zero-field cooling process. The paramagnetic component (cH/T) has been subtracted.

$$\xi^2(0) = \frac{\phi_0}{2\pi \frac{dH_{C2}}{dT} T_c}$$

Both coherence lengths are considerably smaller than the thin-film thickness, suggesting a three-dimensional, nearly isotropic superconductivity.

The superconductivity can only be observed for the $Zn_{1-x}Co_xO$ grown on a Si substrate with the presence of Co-rich nanoparticles and cannot be observed for the $Zn_{1-x}Co_xO$ grown on a SiO_2 substrate. We therefore believe that the superconducting state is directly related to the presence of the Co-rich nanoparticles. Our STEM-EELS measurements reveal the presence, apart from Co^{2+} and Co^{3+} in an O_h symmetry, of Co^{3+} in a trigonal (D_{3d}) symmetry in the Co-rich nanoparticles, which has been observed in Na_xCoO_2.[20,21] We therefore infer that the Co-rich nanoparticles may consist of a core of Co_xO_{1+x} ($1 < x < 4$) surrounded by CoO_2 layers. Consequently, a possible origin of the superconductivity is the presence of Co^{3+} in two-dimensional CoO_2 layers, whose structure is similar to $Na_xCoO_2{\cdot}yH_2O$.[6] Another possibility is that the superconductivity originates from the interface between the Co-rich nanoparticles and the $Zn_{1-x}Co_xO$ matrix, which may be comparable to the superconductivity observed at the interface between two insulating oxides.[8−10] We note that the observed superconductivity cannot be explained by the possible formation of $CoSi_2$, whose T_c (1.2−1.5 K) is much lower than the one we observe in our samples.[22,23]

Finally, although the superconducting transition is evident from the transport measurements in Figure 6a, we do not observe a clear Meissner effect in measurements of the magnetization. We argue that the lack of a strong Meissner effect is due to the fact that the superconductivity remains confined to the Co-rich nanoparticles, implying that the superconducting screening currents may not be well developed.[24,25] Moreover, a weak Meissner effect, if present, can be easily overwhelmed by the dominating influence of the magnetism in the $Zn_{1-x}Co_xO$ matrix and the bulk Si substrate due to the relatively very small volume fraction of superconductivity in $Zn_{1-x}Co_xO$.

Nevertheless, our detailed magnetization measurements on the $Zn_{1-x}Co_xO$ thin film grown on a Si substrate reveal the fingerprints of a diamagnetic response, which we believe to be the result of the weakened Meissner effect. At a magnetic field of 0.1 T, a paramagnetic-like signal shows up (Figure S6(a) in the Supporting Information). We note that a paramagnetic-like signal is also present in the virgin substrate, which is probably due to the highly doped Si. The linear dependence of the magnetization on $1/T$ confirms the paramagnetic behavior, which is probably also influenced by the nonsuperconducting fraction of the $Zn_{1-x}Co_xO$ (Figure S6(b) in the Supporting Information). On the other hand, the deviation at a temperature of around 5 K indicates a decrease of the total magnetization. Therefore, we plot in Figure 6c the temperature dependence of the magnetization after subtracting the paramagnetic component (cH/T, with c being a constant). A decrease of the magnetization (diamagnetic response) is evident at around 5 K, which is consistent with the T_c obtained from transport measurements. The observed fingerprints of the Meissner effect further confirm the presence of superconductivity in our samples on a Si substrate. However, the lack of the strong Meissner effect implies that the superconducting region is very limited in our sample, which, to some extent, favors the interpretation that the observed superconductivity results from the interface between the Co-rich nanoparticles and the $Zn_{1-x}Co_xO$ matrix.

CONCLUSION

We demonstrated unexpected superconductivity with an onset T_c at 5.9 K, which is related to the presence of Co-rich ZnCoO nanoparticles embedded in wurtzite $Zn_{0.7}Co_{0.3}O$ thin films. The superconductivity may result either from the presence of Co^{3+} in two-dimensional CoO_2 layers or from the interface between the Co-rich nanoparticles and the $Zn_{0.7}Co_{0.3}O$ matrix. However, the microstructure of the Co-rich nanoparticles remains to be conclusively determined. Nevertheless, the wurtzite $Zn_{1-x}Co_xO$ provides a new platform for superconductivity, which may be an alternative for the Fe-based superconductors and can benefit from the numerous excellent properties of the ZnO material.

EXPERIMENTAL DETAILS

$Zn_{1-x}Co_xO$ (nominal $x = 0.30 \pm 0.01$) thin films with a thickness of approximately 100 nm were grown by pulsed laser deposition (PLD). Both highly doped Si (100) and Si (100) with a top layer of 300 nm SiO_2 were used as substrates. The energy density per laser pulse was 3 J/cm^2. The growth temperature was 550 °C. The oxygen pressure was maintained at 0.1 Pa during the growth of the $Zn_{1-x}Co_xO$. The crystal structure of the sample was characterized by X-ray diffraction (XRD, PANalytical X'Pert PRO MRD system). The local chemical environment of Co in the sample was characterized by X-ray absorption near

DOI: 10.1021/acsami.5b06363
ACS Appl. Mater. Interfaces 2015, 7, 22166−22171

edge structure (XANES) and extended X-ray absorption fine structure (EXAFS) at the DUBBLE (BM26) beamline of the European Synchrotron Radiation Facility (ESRF). CoO powder and metallic Co foil were used as the reference materials. The microstructure and elemental distribution of the $Zn_{1-x}Co_xO$ were studied by transmission electron microscopy (TEM). A cross-section specimen for TEM was prepared by cutting a thin lamella perpendicular to the film surface using the focused ion beam technique. Energy-filtered transmission electron microscopy (EFTEM) was conducted on a Philips CM30-FEG operated at 300 keV. Energy-dispersive X-ray spectroscopy (EDX) was conducted on a FEI Tecnai G2 microscope operated at 200 keV. Scanning TEM-electron energy loss spectroscopy (STEM-EELS) was conducted on a Titan Cubed microscope operated at 120 keV, which is equipped with an electron monochromator making an energy resolution of 150 meV possible. Multiplet spectra were simulated using the software CTM4XAS version 5.5[17] (related parameters are reported in Table S1, Supporting Information) to determine the absolute valence of Co in the $Zn_{1-x}Co_xO$ matrix and the Co-rich nanoparticles. The electrical contacts for transport measurements were formed by deposition of a Au/Ti bilayer,[26] with a contact area of 0.04 mm^2. The resistivity measurements as a function of temperature were performed in a helium-4 flow cryostat with a superconducting magnet (Oxford Instruments). The magnetic field was applied parallel and perpendicular to the thin-film surface.

■ ASSOCIATED CONTENT

Supporting Information

The Supporting Information is available free of charge on the ACS Publications website at DOI: 10.1021/acsami.5b06363.

Electron diffraction patterns, EFTEM maps, raw EELS map, crystal field and charge transfer parameters as well as results of the fits of the EELS spectra of the Co $L_{2,3}$ edge, temperature dependence of the magnetization (PDF)

■ AUTHOR INFORMATION

Corresponding Authors

*E-mail: yjzeng@szu.edu.cn.

*E-mail: chris.vanhaesendonck@fys.kuleuven.be.

Notes

The authors declare no competing financial interest.

■ ACKNOWLEDGMENTS

This work has been supported by the Research Foundation−Flanders (FWO, Belgium) as well as by the Flemish Concerted Research Action program (BOF KU Leuven, GOA/14/007). N. G. and J. V. acknowledge funding from the European Research Council under the seventh Framework Program (FP7), ERC Starting Grant 278510 VORTEX. The Qu-Ant-EM microscope was partly funded by the Flemish Hercules Foundation. The work at Shenzhen University was supported by National Natural Science Foundation of China under Grant No. 61275144 and Natural Science Foundation of SZU. Y.-J. Z. acknowledges funding under grant no. SKL2015-12 from the State Key Laboratory of Silicon Materials.

■ REFERENCES

(1) Bednorz, J. G.; Muller, K. A. Possible High T_c Superconductivity in the Ba-La-Cu-O System. *Z. Phys. B: Condens. Matter* **1986**, *64*, 189−193.

(2) Kamihara, Y.; Watanabe, T.; Hirano, M.; Hosono, H. Iron-Based Layered Superconductor $La[O_{1-x}F_x]FeAs$ (x = 0.05−0.12) with T_c = 26 K. *J. Am. Chem. Soc.* **2008**, *130*, 3296−3297.

(3) Paglione, J.; Greene, R. L. High-temperature Superconductivity in Iron-based Materials. *Nat. Phys.* **2010**, *6*, 645−658.

(4) Mazin, I. I. Superconductivity Gets an Iron Boost. *Nature* **2010**, *464*, 183−186.

(5) Stewart, G. R. Superconductivity in Iron Compounds. *Rev. Mod. Phys.* **2011**, *83*, 1589−1652.

(6) Takada, K.; Sakurai, H.; Takayama-Muromachi, E.; Izumi, F.; Dilanian, R. A.; Sasaki, T. Superconductivity in Two-dimensional CoO_2 Layers. *Nature* **2003**, *422*, 53−55.

(7) Mizoguchi, H.; Kuroda, T.; Kamiya, T.; Hosono, H. $LaCo_2B_2$: A Co-Based Layered Superconductor with a $ThCr_2Si_2$-Type Structure. *Phys. Rev. Lett.* **2011**, *106* (23), 1−4.

(8) Reyren, N.; Thiel, S.; Caviglia, A. D.; Fitting Kourkoutis, L.; Hammerl, G.; Richter, C.; Schneider, C. W.; Kopp, T.; Rüetschi, A.-S.; Jaccard, D.; Gabay, M.; Muller, D. A.; Triscone, J.-M.; Mannhart, J. Superconducting Interfaces Between Insulating Oxides. *Science* **2007**, *317*, 1196−1199.

(9) Li, L.; Richter, C.; Mannhart, J.; Ashoori, R. C. Coexistence of Magnetic Order and Two-dimensional Superconductivity at $LaAlO_3$/$SrTiO_3$ Interfaces. *Nat. Phys.* **2011**, *7*, 762−766.

(10) Bert, J. A.; Kalisky, B.; Bell, C.; Kim, M.; Hikita, Y.; Hwang, H. Y.; Moler, K. A. Direct Imaging of the Coexistence of Ferromagnetism and Superconductivity at the $LaAlO_3$/$SrTiO_3$ Interface. *Nat. Phys.* **2011**, *7*, 767−771.

(11) Ueno, K.; Nakamura, S.; Shimotani, H.; Ohtomo, A.; Kimura, N.; Nojima, T.; Aoki, H.; Iwasa, Y.; Kawasaki, M. Electric-field-induced Superconductivity in an Insulator. *Nat. Mater.* **2008**, *7*, 855−858.

(12) Ye, J. T.; Inoue, S.; Kobayashi, K.; Kasahara, Y.; Yuan, H. T.; Shimotani, H.; Iwasa, Y. Liquid-gated Interface Superconductivity on an Atomically Flat Film. *Nat. Mater.* **2010**, *9*, 125−128.

(13) Özgür, Ü.; Alivov, Ya. I.; Liu, C.; Teke, A.; Reshchikov, M. A.; Doğan, S.; Avrutin, V.; Cho, S.-J.; Morkoç, H. A Comprehensive Review of ZnO Materials and Devices. *J. Appl. Phys.* **2005**, *98* (4), 041301.

(14) Janotti, A.; Van de Walle, C. G. Fundamentals of Zinc Oxide as a Semiconductor. *Rep. Prog. Phys.* **2009**, *72* (12), 126501.

(15) Li, D. Y.; Zeng, Y. J.; Batuk, D.; Pereira, L. M. C.; Ye, Z. Z.; Fleischmann, C.; Menghini, M.; Nikitenko, S.; Hadermann, J.; Temst, K.; Vantomme, A.; Van Bael, M. J.; Locquet, J.-P.; Van Haesendonck, C. Relaxor Ferroelectricity and Magnetoelectric Coupling in ZnO−Co Nanocomposite Thin Films: Beyond Multiferroic Composites. *ACS Appl. Mater. Interfaces* **2014**, *6*, 4737−4742.

(16) Li, D. Y.; Zeng, Y. J.; Pereira, L. M. C.; Batuk, D.; Hadermann, J.; Zhang, Y. Z.; Ye, Z. Z.; Temst, K.; Vantomme, A.; Van Bael, M. J.; Van Haesendonck, C. Anisotropic Magnetism and Spin-dependent Transport in Co Nanoparticle Embedded ZnO Thin Films. *J. Appl. Phys.* **2013**, *114* (3), 033909.

(17) Stavitski, E.; de Groot, F. M. F. The CTM4XAS Program for EELS and XAS Spectral Shape Analysis of Transition Metal L Edges. *Micron* **2010**, *41*, 687−694.

(18) Pfleiderer, C.; Uhlarz, M.; Hayden, S. M.; Vollmer, R.; Lohneysen, H. v.; Bernhoeft, N. R.; Lonzarich, G. G. Coexistence of Superconductivity and Ferromagnetism in the *d*-band Metal $ZrZn_2$. *Nature* **2001**, *412*, 58−61.

(19) Tinkham, M. *Introduction to Superconductivity*, 2nd ed; McGraw-Hill, Inc.: New York, 1996.

(20) Kroll, T.; Aligia, A. A.; Sawatzky, G. A. Polarization Dependence of X-ray Absorption Spectra of Na_xCoO_2: Electronic Structure from Cluster Calculations. *Phys. Rev. B: Condens. Matter Mater. Phys.* **2006**, *74* (11), 115124 .

(21) Lin, H.-J.; Chin, Y. Y.; Hu, Z.; Shu, G. J.; Chou, F. C.; Ohta, H.; Yoshimura, K.; Hébert, S.; Maignan, A.; Tanaka, A.; Tjeng, L. H.; Chen, C. T. Local Orbital Occupation and Energy Levels of Co in Na_xCoO_2: A Soft x-ray Absorption Study. *Phys. Rev. B: Condens. Matter Mater. Phys.* **2010**, *81* (11), 115138.

(22) Matthias, B. T.; Hulm, J. K. Superconducting Properties of Cobalt Disilicide. *Phys. Rev.* **1953**, *89*, 439−441.

(23) White, A. E.; Short, K. T.; Dynes, R. C.; Garno, J. P.; Glbson, J. M. Mesotaxy: Single-crystal Growth of Buried $CoSi_2$ Layers. *Appl. Phys. Lett.* **1987**, *50*, 95−97.

DOI: 10.1021/acsami.5b06363
ACS Appl. Mater. Interfaces 2015, 7, 22166−22171

(24) Mastellone, A.; Falci, G.; Fazio, R. Small Superconducting Grain in the Canonical Ensemble. *Phys. Rev. Lett.* **1998**, *80*, 4542−4545.
(25) von Delft, J. Superconductivity in Ultrasmall Metallic Grains. *Ann. Phys. (Berlin, Ger.)* **2001**, *10*, 219−276.
(26) Zeng, Y. J.; Pereira, L. M. C.; Menghini, M.; Temst, K.; Vantomme, A.; Locquet, J.-P.; Van Haesendonck, C. Tuning Quantum Corrections and Magnetoresistance in ZnO Nanowires by Ion Implantation. *Nano Lett.* **2012**, *12*, 666−672.

DOI: 10.1021/acsami.5b06363
ACS Appl. Mater. Interfaces 2015, 7, 22166−22171